Physicochem. Probl. Miner. Process., 56(4), 2020, 723-736

http://www.journalssystem.com/ppmp

Physicochemical Problems of Mineral Processing

ISSN 1643-1049

Received May 03, 2020; reviewed; accepted June 29, 2020

Effect of the degree of polymerization of nonylphenol polyoxyethylene ether on the dewatering of low-rank coal

Lin Li [1], Meng He [1], Mingpu Liu [1], Mengyu Lin [1], Shanpei Hu [1], Hao Yu [1], Qingbiao Wang [2], Xiaofang You [1]

[1] College of Chemical and Environmental Engineering, Shandong University of Science and Technology, Qingdao, Shandong 266590, China

[2] National Engineering Laboratory for Coalmine Backfilling Mining, Shandong University of Science and Technology, Tai'an, Shandong 271019, China

Corresponding author: youxiaofang1212@sdust.edu.cn (Xiaofang You)

Abstract: In this study, we investigated the effect of the hydrophilic ethylene oxide chain lengths (i.e., degree of polymerization) of nonylphenol polyoxyethylene ether (NPEO-x, x = 8, 10, and 12) on the dewatering of low-rank coal slime through dewatering and adsorption experiments and X-ray photoelectron spectroscopy (XPS) measurements. The dewatering experiments showed that the adsorption of NPEO changed the water content of the low-rank coal slime: NPEO-8 achieved the best effect, followed, in decreasing order, by NPEO-10 and NPEO-12. Adsorption experiments revealed that the adsorption isotherms of NPEO-x on the low-rank coal surface conform with the Langmuir model, and its adsorption kinetics follow the pseudo-second-order kinetic equation. Furthermore, the adsorption is a spontaneous process and controlled by both intraparticle diffusion and liquid film diffusion. The XPS results showed that the adsorption of NPEO-x decreased the content of oxygen-containing groups and, thus, improved the hydrophobicity of the low-rank coal surface. Further, the use of NPEO-x with a low degree of polymerization (x = 8) improves the hydrophobicity of the coal surface and decreases the water content of low-rank coal slime.

Keywords: low-rank coal, NPEO, dewatering, adsorption, long-flame coal

1. Introduction

Moisture is an important factor in coal processing, affecting the calorific value and utilization rate of the coal combustion process. Tao et al. reported that, if the moisture of a typical North American coal were reduced by 1%, the calorific value of the fuel would be increased by 1.4% (Tao et al., 2000). Thus, the dewatering of fine coal is crucial.

Long-flame coal is a typical type of low-rank coal and is an important part of China's coal energy resources. Compared with bituminous coal, low-grade coal has higher inherent moisture, and this is even higher when in contact with water (Vaziri Hassas et al., 2014; X. Zhu et al., 2020). This water content depresses the calorific value achieved during combustion, resulting in energy waste. Mechanical dewatering, thermal dewatering, and composite dewatering technology are common methods for the removal of water from fine coal particles, and the residual moisture content of fine coal is approximately 25% after mechanical dewatering (Le Roux et al., 2005). Consequently, these products can require further dewatering, which increases processing costs (Yoon et al., 2004). Thermal dewatering has been recommended to remove water from fine particles (Bergins et al., 2007; Hulston et al., 2005; Vogt et al., 2012), but this process is costly and environmentally damaging. There are many forms of composite dewatering technology. Groppo and coworkers (Groppo and Parekh, 1996) studied continuous pressure filtration with surfactants for the dewatering of fine coal. The results indicated that both nonionic and cationic surfactants effectively reduce the moisture in the filter cake to less than 20% at dosages as low

DOI: 10.37190/ppmp/124767

as 0.25 kg/t. Vacuum filtration of clean coal slurry and flocculated slurry with cationic, anionic, and nonionic surfactants was investigated by Singh (Singh et al., 1998). For all types of surfactant, the moisture content of the filter cake was significantly reduced, and the most effective surfactant type was cationic. Therefore, the combination of mechanical dewatering and filtrating is very effective.

Surfactants have amphiphilic molecular structures and can effectively adsorb on the coal surface; thus, they can be used to adjust the wettability of the coal surface. In some investigations, surfactants have been shown to improve the hydrophobicity of coal surface (Ahmet et al., 1995; X. Liu et al., 2017; You, He, Zhu, et al., 2019) and reduce the moisture content of the filter cake (Singh, 1997, 1999; StrohandStahl, 1990; Vaziri Hassas et al., 2014). The dewatering of flotation coal concentrates with different degrees of fineness was investigated by Stroh (StrohandStahl, 1990) using nonionic alkyl-polyalkylene oxides and anionic sulfosuccinate surfactants. The results showed that the moisture content significantly decreased at surfactant concentrations close to the critical micelle concentration (CMC). The dewatering of lignite and sub-bituminous and bituminous coal was studied by Hassas (Vaziri Hassas et al., 2014) using Triton-X series surfactants and three other reagents that had the same hydrophobic–lipophilic balance (HLB) value. It was found that, for the fine particles with lower hydrophobicity, such as lignite and subbituminous coals, surfactants with higher HLB values (about 10) achieved the optimum dewatering. Further, it was found that there is an optimal concentration for each reagent, and the moisture content of the filter cake increases in case of the concentration above.

The aim of this study is to investigate the relationship between the degree of polymerization (x = 8, 10, and 12) of nonylphenol surfactants (nonylphenol polyoxyethylene ether (NPEO)) and long-flame coal. Dewatering experiments, adsorption experiments, and X-ray photoelectron spectroscopy (XPS) measurements were carried out to reveal the effect of the hydrophilic ethylene oxide chain lengths on the dewatering effect of long-flame coal slime.

2. Materials and methods

2.1. Coal samples

Coal samples were obtained from the Shendong mining area. The samples were all long-flame coal, a typical low-rank coal. The samples were prepared for experiments according to the international standard MT/T808-1997 and were packed in sealed bags and placed in a dry environment.

The experimental coal sample was ground to 200 meshes, and vacuum dried at 50 °C for 1 h. Proximate analysis and ultimate analysis were carried out according to GB/T 212-2008, GB/T 213-2008, GB/T 214-2007, GB/T 476-2008 and GB/T 19227-2008. Table 1 shows the proximate analysis and the ultimate analysis of the coal sample. The ash content of the sample is 21.60%, the volatile matter is 37.90%, and the fixed carbon is 62.10%, which is a long flame coal. The elemental analysis of the coal sample indicates that the contents of carbon, oxygen and hydrogen are 79.49%, 14.22% and 4.75%, respectively.

Table 1. Proximate and ultimate analysis of long flame coal

Proximate Analysis[a] (%)				Ultimate Analysis$_{daf}$ (%)				
M_{ad}	A_d	V_{daf}	FC_{daf}	C	H	N	O[b]	S
7.29	21.60	37.90	62.10	79.49	4.75	0.57	14.22	0.97

[a] M_{ad} is moisture on an air-dried basis, A_d is ash content on a dried basis, V_{daf} and FC_{daf} are volatile matter and fixed carbon on a dried ash free basis, respectively

[b] Subtraction Calculation

The X-ray diffraction (XRD) patterns of the raw coal samples are shown in Fig. 1 (black line). By comparing the standard XRD patterns, we found that the raw coal sample contains quartz, calcite, and a small amount of kaolinite, which would interfere with the experimental results and severely affect the coal analysis. Therefore, the coal samples required demineralization.

To reduce the experimental error, demineralization using a mixture of HF, HCl, and distilled water was used to remove the gangue minerals from the raw coal (Hao et al., 2013). The XRD pattern of the sample after demineralization is shown in Fig. 1 by a red line. As shown, the reflections corresponding to quartz, calcite, and kaolinite impurity minerals are absent after demineralization, which should reduce any interference of impurity minerals on the experimental results.

The NPEO was obtained from Union Carbide Corporation, which purity ≥ 99%. Chemical structure formula of NPEO is revealed in Fig. 2.

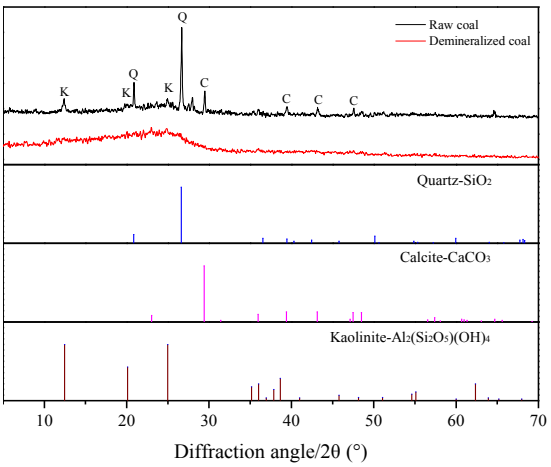

Fig. 1. XRD patterns of raw and demineralized coal

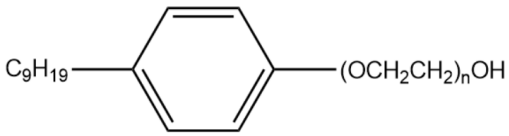

Fig. 2. Structure formula of NPEO (n=8,10,12)

2.2. Experimental methods

2.2.1. Dewatering experiment

A series of NPEO-x samples with different degrees of polymerization (x = 8, 10, or 12) solutions were prepared in different concentrations. Then, 25 mL of each solution was transferred to 100-mL Erlenmeyer flasks containing 2.00 g coal sample. The mixture was shaken at 120 rad/min in a constant temperature water bath at 30 °C for 10 h. A vacuum sampler was used to separate the coal sample from the solution, and the coal samples were placed in a blast drying box at 60 °C for 8 h until dried to a constant weight. The water content of the coal samples was calculated using Eq. (1).

$$\omega = \frac{(m_1 - m_2)}{m_1} \times 100\% \quad (1)$$

Here, ω is the water content of coal samples (%), m_1 is the weight of coal samples that separate from the solution (g), and m_2 is the weight of coal samples after drying (g).

2.2.2. Adsorption experiments

For these experiments, 25 mL of NPEO solution (several concentrations were tested) was added to a 100-mL conical flask containing a fixed amount of coal sample (0.5000 ± 0.001 g), then the flasks were agitated in a water bath shaker at 25, 35, or 45 °C for 24 h. The solutions after adsorption were obtained by vacuum filtration, and, then, the equilibrium concentrations of NPEO were determined using ultraviolet–visible spectroscopy. The amount of NPEO adsorbed on coal surface was calculated using Eq. (2) (ŞahinandEmik, 2018; You, He, Cao, et al., 2019).

$$q_e = \frac{(c_0 - c_e) \cdot V}{m} \quad (2)$$

Here, c_0 is the initial concentration of NPEO (mg/L), c_e is the equilibrium concentration of NPEO (mg/L), q_e is the amount of NPEO adsorbed by the coal at equilibrium (mg/g), V is the volume of the solution (L), and m is the mass of the coal sample (g).

2.2.3. X-ray photoelectron spectroscopy

XPS (ESCALAB 250Xi) measurements were used to analyze the elemental content of the coal surface. The XPS system was equipped with a monochromatic Al (K_α) X-ray source and operated at 200 W. A pass energy of 150 eV was applied for the elemental scan with a step size of 0.05 eV, and the vacuum of the analytical chamber exceeded 1×10^{-9} Pa. The C1s spectrum was recorded in constant analyzer energy (CAE) mode with 20 eV pass energy.

3. Results and discussion

3.1. Dewatering experiments

Fig. 3 shows the change in water content of long-flame coal with increase in NPEO concentration. As shown in the figure, the water content of the coal samples varies with the equilibrium concentration of the three NPEO samples. The trends in the water content of the coal samples are similar, all decreasing at first and then increasing. These results reveal that the wettability of long-flame coal surface can be adjusted by changing the concentration of NPEO.

Compared with the original sample, the water content of the long-flame coal sample decreased after adsorbing NPEO-8, NPEO-10, and NPEO-12, reaching minimum values at the absorptive capacity of 1.66×10^{-5}, 1.41×10^{-5}, and 1.21×10^{-5} mol/g, respectively, and the water contents decreased by 8.72%, 7.50%, and 5.64%, respectively, for these NPEO samples. Thus, NPEO-8 shows the best dewatering effect, followed by those of NPEO-10 and NPEO-12 in decreasing order. Moreover, the dewatering effect is best when the NPEO concentration approaches the critical micelle concentration CMC.

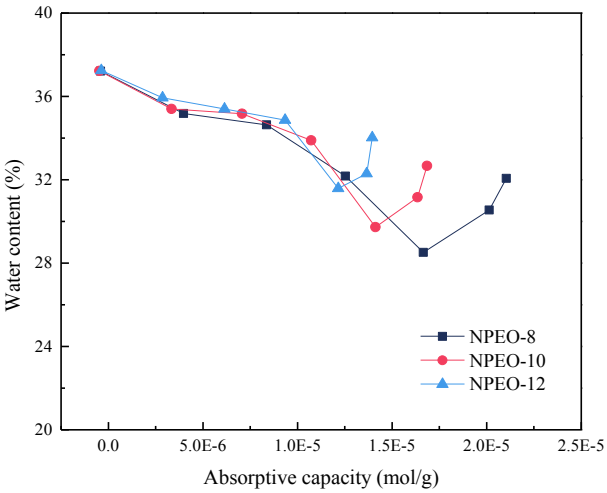

Fig. 3 Effects of NPEO adsorption on water content of long-flame coal

3.2. Adsorption experiments

The isothermal adsorption curves (Fig. 4) of NPEO on each coal sample were obtained by adsorption experiments. The adsorption isotherms were L-type; that is, the amount of NPEO adsorbed on the coal surface increases with increase in concentration, gradually levelling off at higher concentrations. The adsorption isotherms of NPEO-8, NPEO-10, and NPEO-12 on the low-rank coal surface are similar. When the equilibrium concentration of NPEO-8, NPEO-10 and NPEO-12 in the solution was about 38.17mg/L, 54.16mg/L and 72.48mg/L, respectively, the inflection point appeared in the adsorption curve. Moreover, the maximum adsorption capacity of NPEO increased with increasing temperature. For example, the maximum adsorption capacity of NPEO-8 was 26mg/g, 31mg/g, and 36mg/g at 25, 35, and 45℃, respectively, indicating increasing temperature was favorable to the adsorption of NPEO on low rank coal surface. Furthermore, the maximum adsorption capacity of NPEO-8, NPEO-10 and

NPEO-12 were 26mg/g, 24mg/g, and 21mg/g severally at 25℃, showing that the maximum adsorption capacity decreased with increase in degree of polymerization (8 → 12). This is because the interaction between NPEO and water increases with increase in degree of polymerization, but the interaction between NPEO and coal decreases (SisandChander, 2003).

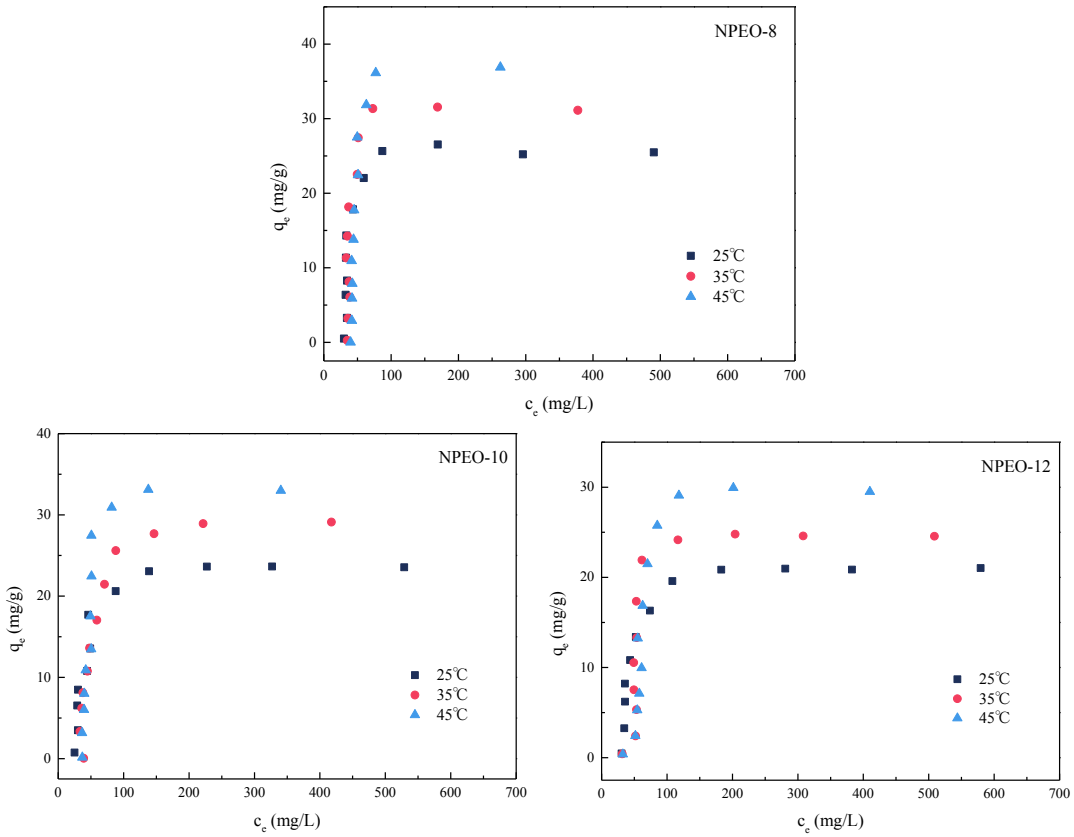

Fig. 4 Adsorption isotherms of NPEO on low-rank coal

3.2.1. Adsorption isotherms

The Langmuir and Freundlich models were used to analyze the adsorption isotherms. The Langmuir model (Cheng et al., 2014; VadivelanandKumar, 2005; Xu et al., 2013) is given by Eq. (3).

$$\frac{q_e}{q_m} = \frac{K_L c_e}{1+K_L c_e} \tag{3}$$

The linear form of Eq. (3) is given by Eq. (4) (Lyu et al., 2018).

$$\frac{c_e}{q_e} = \frac{c_e}{q_m} + \frac{1}{K_L q_m} \tag{4}$$

Here, c_e is the equilibrium concentration of NPEO (mg/L), q_e is the amount of NPEO adsorbed by the coal at equilibrium (mg/g), q_m is the maximum amount of NPEO adsorbed by coal (mg/g), and K_L is the Langmuir isotherm constant.

The Freundlich model is given by Eq. (5) (HameedandEl-Khaiary, 2008b).

$$q_e = K_F \cdot c_e^n \tag{5}$$

The linear form of Eq. (5) is given by Eq. (6) (Saha et al., 2005; You, He, Cao, et al., 2019).

$$\log q_e = n \cdot \log c_e + \log K_F \tag{6}$$

Here, K_F is the Freundlich equation constant ($(mg \cdot g^{-1}) \cdot (L \cdot mg^{-1})^{1/n}$), which is related to the adsorption capacity, and n is the characteristic adsorption constant, which relates to the adsorption intensity.

The fitted parameters for the Langmuir and Freundlich models are listed in Table 2. The coefficient of determination (R^2) for the fitting to the Langmuir model is obviously higher than that of the Freundlich model, indicating the adsorption of NPEO on low-rank coal can be described best by the Langmuir isotherm. The maximum adsorption capacity of NPEO-8 NPEO-10 and NPEO-12 on low rank

coal surface was 26.08, 24.29, and 21.65 mg/g severally at 25℃, which was very close to the equilibrium adsorption capacity. Other temperatures as well.

Table 2. Fitted adsorption parameters for NPEO on coal samples

Surfactant	T, ℃	Langmuir			Freundlich		
		q_m, mg/g	K_L, L/g	R^2	K_F	n	R^2
NPEO-8	25	26.08	117.41	0.9995	0.030	0.11	0.3972
	35	31.25	172.49	0.9998	0.033	0.07	0.2020
	45	36.04	202.58	0.9999	0.037	0.05	0.2605
NPEO-10	25	24.29	83.64	0.9999	0.027	0.12	0.7300
	35	28.85	112.68	0.9996	0.031	0.09	0.4120
	45	33.88	137.98	0.9999	0.034	0.05	0.5608
NPEO-12	25	21.65	71.93	0.9995	0.023	0.10	0.5529
	35	25.34	85.95	0.9995	0.028	0.12	0.4679
	45	29.51	115.86	0.9996	0.031	0.08	0.2833

3.2.2. Adsorption thermodynamics

The corresponding thermodynamic parameters were calculated using Eqs. (7-9). The change in the free energy (ΔG) is given by Eq. (7) (Demirbas et al., 2006; Pedro Silva et al., 2004; You et al., 2018).

$$\Delta G = -\mathrm{R}T \cdot \ln K \tag{7}$$

The enthalpy change (ΔH) is given by the Clausius–Clapeyron equation, as shown in Eq. (8) (S. Liu et al., 2020; Y. Liu, 2009).

$$\ln \mathrm{K} = -\frac{\Delta H}{\mathrm{R}T} + \frac{\Delta S}{\mathrm{R}} \tag{8}$$

The entropy change (ΔS) is given by Eq. (9).

$$\Delta G = \Delta H - T\Delta S \tag{9}$$

In Eqs. (7-9), T is the temperature (K), R is the ideal gas constant (8.314J/(mol·K)), and K is the thermodynamic equilibrium constant, which is given by the Langmuir isotherm equation. The thermodynamic parameters for adsorption are listed in Table 3.

Table 3. Thermodynamic parameters for the adsorption of NPEO on low-rank coal

Surfactant	T, ℃	ΔG, kJ/mol	ΔH, kJ/mol	ΔS, J·K^{-1}·mol^{-1}
NPEO-8	25	-27.54	21.58	164.82
	35	-29.45	21.58	95.61
	45	-30.83	21.58	96.94
NPEO-10	25	-27.05	19.75	157.06
	35	-28.72	19.75	93.26
	45	-30.19	19.75	94.94
NPEO-12	25	-26.99	18.72	153.38
	35	-28.35	18.72	92.05
	45	-30.06	18.72	94.53

The negative sign of the free energy (ΔG) for the adsorption of NPEO on low-rank coal in the range of studied temperatures suggests that adsorption was a spontaneous reaction and thermodynamically favorable (Oyelude et al., 2017). Moreover, the absolute values of ΔG were between 25 to 31 kJ/mol, which indicated that the adsorption of NPEO on long-flame coal was physical absorption (B. ZhuandZhao, 1999). The positive value of ΔH implies that adsorption is an endothermic adsorption

process. In addition, the value of ΔS was greater than zero, which reflects the increased randomness at the coal–NPEO solution interface (Oyelude et al., 2017; Sun et al., 2008).

A higher absolute value of ΔG implies a more energetically favorable adsorption process. The values of ΔG adsorbed by NPEO-8, NPEO-10, and NPEO-12 on low rank coal surface were -27.54kJ/mol, -27.05kJ/mol and -26.99kJ/mol at 25℃, respectively, showing that the absolute values of ΔG adsorbed by NPEO-8, NPEO-10, and NPEO-12 on the low-rank coal surface decreased with increase in the number of ethylene oxide units, which indicated that a lower degree of polymerization is favorable for the adsorption of NPEO on the low-rank coal surface.

3.2.3. Adsorption kinetics

Pseudo-first-order and pseudo-second-order kinetic models were used to study the adsorption of NPEO on the low-rank coal surface.

The pseudo-first-order kinetic model is given by Eq. (10) (VadivelanandKumar, 2005).

$$\frac{\mathrm{d}q_\mathrm{t}}{\mathrm{d}t} = \mathrm{K}_1 \cdot (q_\mathrm{e} - q_\mathrm{t}) \tag{10}$$

The linear formula of Eq. (10) after integration is given by Eq. (11) (ŞahinandEmik, 2018).

$$\ln(q_\mathrm{e} - q_\mathrm{t}) = \ln q_\mathrm{e} - \mathrm{K}_1 t \tag{11}$$

Here, q_e is the amount NPEO adsorbed by the coal at time t in the adsorption process (mg/g), and K_1 is the pseudo-first-order rate constant.

The pseudo-second-order kinetic model is given by Eq. (12) (VadivelanandKumar, 2005; Xiao et al., 2020).

$$\frac{\mathrm{d}q_\mathrm{t}}{\mathrm{d}t} = \mathrm{K}_2 \cdot (q_\mathrm{e} - q_\mathrm{t})^2 \tag{12}$$

The linear formula after integration is given by Eq. (13) (Oyelude et al., 2017).

$$\frac{t}{q_\mathrm{t}} = \frac{1}{\mathrm{K}_2 q_\mathrm{e}^2} + \frac{t}{q_\mathrm{e}} \tag{13}$$

Here, K_2 represents the pseudo-second-order rate constant.

The adsorption kinetics curves of NPEO on low-rank coal at different contact times are shown in Fig. 5, and the adsorption curves are all very similar. The amount of NPEO adsorbed by the coal increased rapidly in the first 60 min; after this, the increase slowed; finally, equilibrium was reached after 720 min.

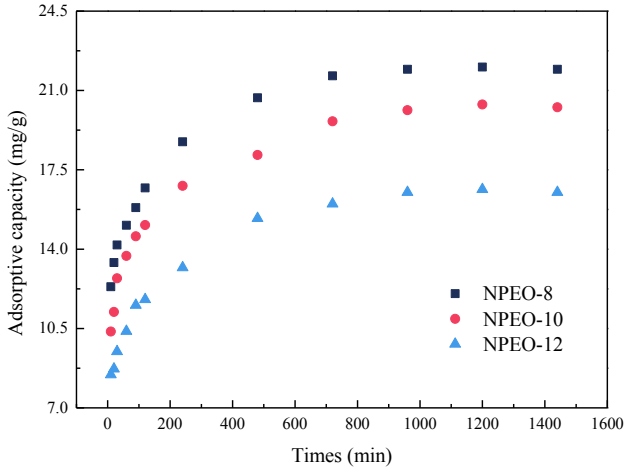

Fig. 5. Adsorption kinetic curves of NPEO on coal samples

The fitting parameters for the pseudo-first-order and pseudo-second-order models are listed in Table 4. The values of R^2 achieved using the pseudo-second-order model are obviously higher than those obtained with the pseudo-first-order model, and, for the second-order model, the theoretical adsorption capacities (q_{e2}) are very close to the maximum equilibrium adsorption capacities obtained by experiment. This indicates that the adsorption of NPEO on low-rank coal fitted the pseudo-second-order kinetic model best.

Table 4. Kinetic parameters for the adsorption of NPEO on low-rank coal

Surfactant	q_e, mg/g	Pseudo-first-order			Pseudo-second-order		
		q_{e1}, mg/g	K_1	R^2	q_{e2}, mg/g	K_2	R^2
NPEO-8	25.32	8.04	0.0018	0.8924	22.40	1.622	0.9994
NPEO-10	24.04	8.14	0.0020	0.9406	20.69	1.463	0.9988
NPEO-12	20.79	7.03	0.0023	0.9334	16.96	1.618	0.9988

3.2.4. Adsorption diffusion mechanism

The intraparticle diffusion and film diffusion models are the two most widely used models to identify the limiting adsorption step of the adsorption process.

The intraparticle diffusion model is given by Eq. (14) (Caceres-Jensen et al., 2013; HameedandEl-Khaiary, 2008b; Hameed et al., 2009).

$$q_t = K_{id} \cdot t^{0.5} + C \tag{14}$$

Here, K_{id} is the intraparticle diffusion constant, and C is an arbitrary constant.

If, on fitting Eq. (14), a linear fit is obtained and C is zero, then intraparticle diffusion is the sole rate-limiting step. Otherwise, there is likely another rate-limiting step involved.

The film diffusion model (Ahamad et al., 2018; TaffarelandRubio, 2009) is given by Eq. (15).

$$\ln(1 - F) = -K_{fd} \cdot t \tag{15}$$

Here, F is the ratio of the adsorption capacities at time t and equilibrium ($F = q_t/q_e$), and K_{fd} is the adsorption rate constant.

On fitting the data to Eq. (15), if a zero intercept is obtained, the adsorption kinetics is controlled by diffusion through the liquid film surrounding the solid sorbent. Otherwise, film diffusion is not only the rate-limiting step, and intraparticle diffusion could also be taking place.

The Boyd model can be used to identify whether external transport or intraparticle transport (i.e., film diffusion or intraparticle diffusion) control the rate of adsorption (Eq. (16)) (Caceres-Jensen et al., 2013; Onal et al., 2007).

$$(1 - F) = \frac{6}{\pi^2} e^{-Bt} \tag{16}$$

Here, $F = q_t/q_e$, and Bt is a function of F.

If $F < 0.85$, Bt is given by Eq. (17) (HameedandEl-Khaiary, 2008a).

$$Bt = \left(\sqrt{\pi} - \sqrt{\pi - \left(\frac{\pi^2 F}{3}\right)}\right)^2 \tag{17}$$

If $F > 0.85$, Bt is given by Eq. (18) (Caceres-Jensen et al., 2013; HameedandEl-Khaiary, 2008a).

$$Bt = -0.4977 - \ln(1 - F) \tag{18}$$

If the regression of Bt versus t is a straight line with zero intercept, the adsorption rate is governed by the intraparticle diffusion mechanism. If the fit is nonlinear or linear but does not pass through the origin, film diffusion or chemical reaction controls the adsorption rate.

The experimental data were fitted to the Weber–Morris equation. As shown in Fig. 6, there are two linear portions. At the beginning of adsorption, there is a linear region representing pore diffusion, followed by a horizontal linear region representing equilibrium. The slope and intercept of the second linear portion characterize the rate of intraparticle diffusion; these parameters are listed in Table 5.

From Table 5, the R^2 values of the fitted curve of q_t versus $t^{0.5}$ are all higher than 0.9, but the intercept C values are not zero; that is, the straight line does not pass through the origin, suggesting intraparticle diffusion is not the sole rate-limiting step in the adsorption of NPEO on low-rank coal. Fitting to the film diffusion model yielded straight lines that did not pass through the origin, indicating that film diffusion is not the only rate-limiting step. Therefore, the adsorption of NPEO on low-rank coal surface is controlled by both liquid film diffusion (external mass transfer) and intraparticle diffusion (mass transfer through the pores). The Bt values were plotted against time following the Boyd model, as shown in Fig. 7, and the results are presented in Table 6. The values of R^2 are all greater than 0.9,

indicating that the plot of Bt versus *t* (the initial stage of adsorption) is linear; however, the linear plot does not pass through the origin, indicating that the adsorption rate of NPEO on low-rank coal is governed by film diffusion.

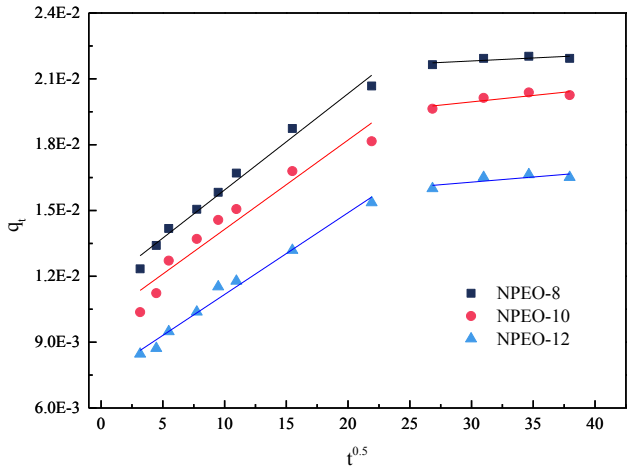

Fig. 6. Fitting of the adsorption of NPEO on coal samples to the intraparticle diffusion model

Table 5. Results of fitting to intraparticle and liquid film diffusion model

Surfactant	Intraparticle diffusion			Liquid film diffusion		
	K_{id}	C	R^2	K_{fd}	A	R^2
NPEO-8	0.00044	0.012	0.9794	0.0018	-1.05	0.8924
NPEO-10	0.00041	0.010	0.9196	0.0020	-0.95	0.9406
NPEO-12	0.00037	0.007	0.9817	0.0023	-0.88	0.9334

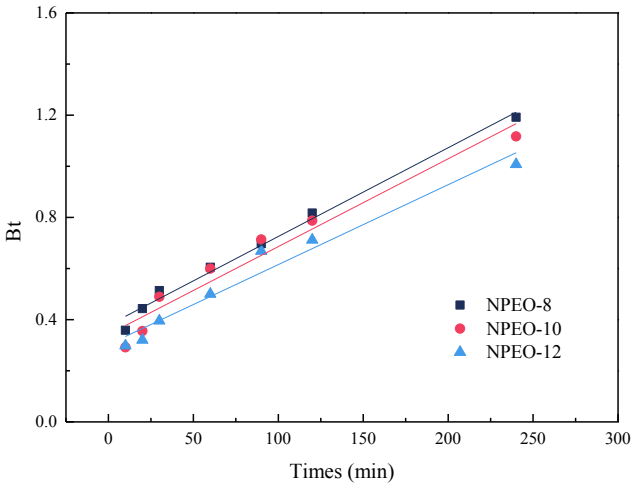

Fig. 7. Fitting of the liquid film diffusion of NPEO on low-rank coal

3.3. FTIR analysis

The transmittance intensity of peaks near 3690 cm^{-1} (-OH group) and 910 cm^{-1}(Si-O-Si group) in the spectrum of raw long-flame coal was slightly higher than that in the spectrum of long-flame coal after adsorbing NPEO. These results showed that long-flame coal after adsorbing NPEO has slightly higher hydrophobic properties than raw coal. Comparing the samples which adsorbing NPEO could be found that the transmittance intensity variation of peaks is tiny, resulting in an inability to determine which effect is better. Therefore, the XPS was used for further study.

Table 6. Results of fitting to the Boyd model

Surfactant	Slope	Intercept	R^2
NPEO-8	0.0035	0.38	0.9867
NPEO-10	0.0034	0.34	0.9441
NPEO-12	0.0031	0.30	0.9580

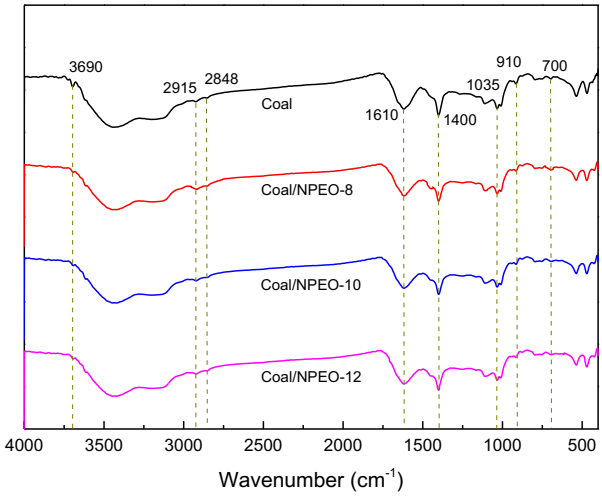

Fig. 8. The FTIR spectra of samples

3.4. XPS analysis

XPS analysis of the low-rank coal surface was carried out, and the elemental contents were calculated assuming the sum of the C, O, Si, and Al content to be 100%. The relative content of C, O, Si, and Al on the low-rank coal surface with or without surfactant is different (Fig. 9), and the atomic contents are listed in Table 7.

Compared to that of low-rank coal without NPEO, the C content on low-rank coal with NPEO-8, NPEO-10, and NPEO-12 increased by 1.96%, 1.44%, and 1.08%, respectively, whereas the O content decreased from 17.16% to 15.25%, 15.83%, and 16.16%. This shows that NPEO had adsorbed onto the low-rank coal surface.

Peak fitting and deconvolution of the C1s peak was performed using XPS Peak 4.1, and the fitting curves are shown in Fig. 10. The C-C/C-H, -COOH, >C=O, and -C-O contents were calculated from the

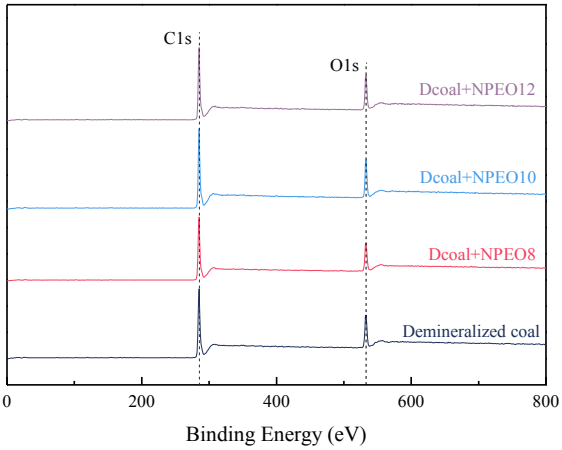

Fig. 9. XPS wide energy scans of the demineralized coal surface before and after the adsorption of NPEO

fitting results, and the contents of the carbon-containing groups on each coal sample (demineralized coal surface with and without NPEO) are listed in Table 8.

As shown by Table 8, the C-C/C-H group content on the samples surface increased by 5.26%, 3.21%, and 1.80% after the adsorption of NPEO-8, NPEO-10, and NPEO-12, respectively. Moreover, the C-O, C=O, and O=C-O contents on the sample surfaces all decreased after the adsorption of NPEO. This indicates that NPEO was adsorbed on the low-rank coal surface, and this improved the hydrophobicity of the coal surface and enhanced the dewatering of the low-rank coal. On the basis of the peak fitting of the C1s peak in the spectra of the coal surface after the adsorption of NPEO, the greatest increase in C-C/C-H content was that for NPEO-8, followed, in decreasing order, by those for NPEO-10 and NPEO-12. This shows that NPEO-8 improved the hydrophobicity of the coal surface to the greatest extent, which is consistent with the results of dewatering experiments.

Table 7. Contents of C1s, O1s, Si2p, and Al2p on demineralized coal surface before and after adsorbing NPEO

Sample	Element content, %			
	C1s	O1s	Si2p	Al2p
Demineralized coal	81.76	17.16	0.55	0.53
Dcoal/NPEO-8	83.71	15.25	0.47	0.56
Dcoal/NPEO-10	83.19	15.83	0.45	0.53
Dcoal/NPEO-12	82.84	16.16	0.49	0.51

Dcoal is logogram of demineralized coal

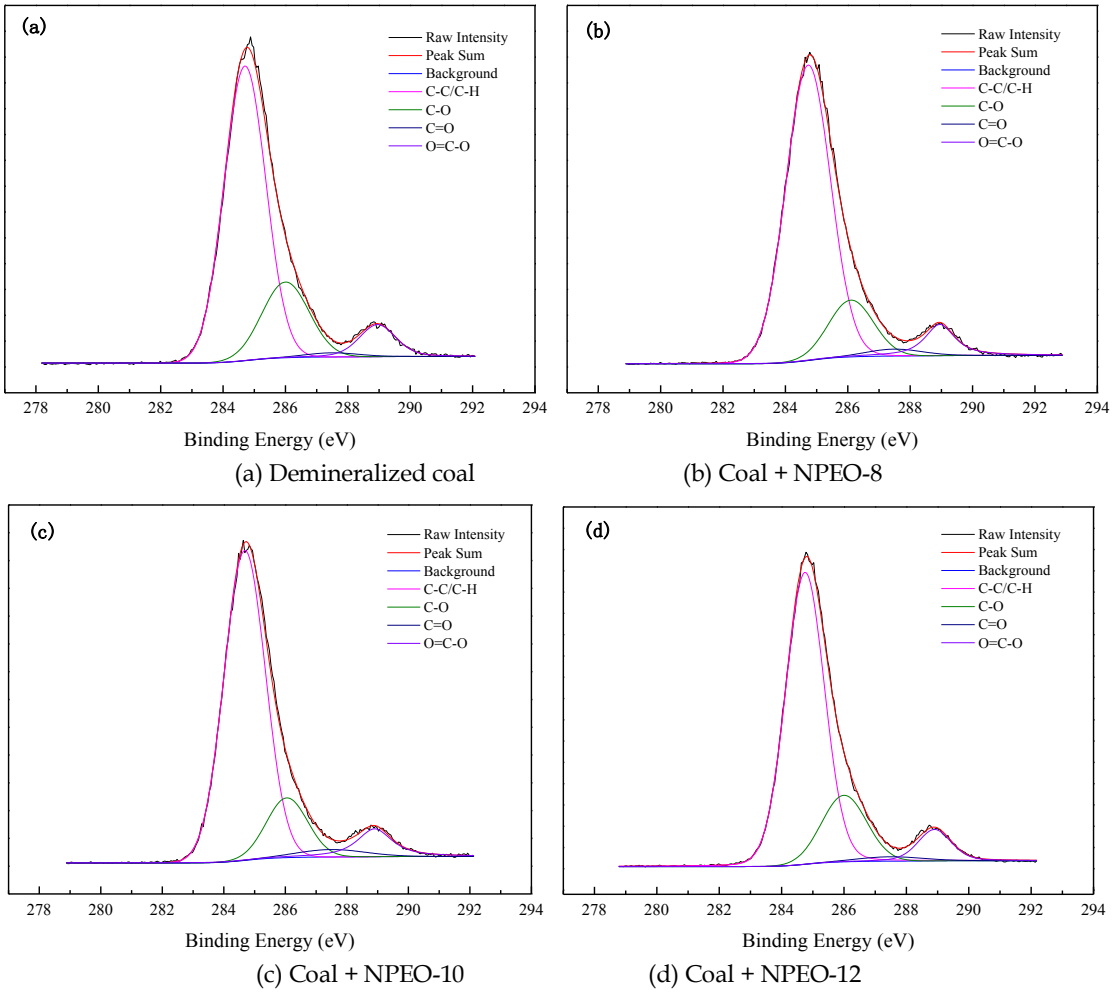

(a) Demineralized coal (b) Coal + NPEO-8

(c) Coal + NPEO-10 (d) Coal + NPEO-12

Fig. 10 Peak fitting of C1s peaks on coal samples

Table 8. Content of carbon-containing groups on coal samples

Sample	Content, %			
	C-C/C-H	C-O	C=O	O=C-O
Demineralized coal	70.69	20.46	1.27	7.58
Dcoal/NPEO-8	75.95	14.51	2.19	7.35
Dcoal/NPEO-10	73.90	15.71	2.76	7.62
Dcoal/NPEO-12	72.49	18.48	1.74	7.29

4. Conclusions

The following conclusions were obtained. The water contents of long-flame coal samples after the adsorption of NPEO-8, NPEO-10, and NPEO-12 reached 38.17, 54.16, and 72.48 mg/L, representing decreases of 8.72%, 7.50%, and 5.64%, respectively. This indicates that NPEO-8 has the best dewatering effect for low-rank coal, followed, in decreasing order, by NPEO-10 and NPEO-12. The adsorption isotherms of NPEO on low-rank coal were best described by the Langmuir model, and the adsorption kinetics fit the pseudo-second-order kinetic equation well. Moreover, the adsorption process was controlled by both intraparticle diffusion and liquid film diffusion, and film diffusion controls the adsorption rate. The adsorption of NPEO on low-rank coal is a spontaneous endothermic process and is governed by physical adsorption. The contents of C-C/C-H groups on the sample surfaces increased after the adsorption of NPEO, whereas the surface contents of C-O, C=O, and O=C-O groups decreased. Moreover, the largest increase in C-C/C-H content was observed after the treatment of the coal with NPEO-8, followed in decreasing order by NPEO-10 and NPEO-12, indicating that NPEO-8 resulted in the greatest increase in the hydrophobicity of the coal surface.

Acknowledgments

This work was supported by Shandong Province Key Research and Development Project (2019GGX103035), National Natural Science Foundation of China (51904174), Young Science and Technology Innovation Program of Shandong Province (2020KJD001), Project of Shandong Province Higher Educational Young Innovative Talent Introduction and Cultivation Team [Hydrogen energy chemistry innovation team], and SDUST Research Fund (2018TDJH101).

References

AHAMAD, K. U., SINGH, R., BARUAH, I., CHOUDHURY, H., SHARMA, M. R., 2018. *Equilibrium and kinetics modeling of fluoride adsorption onto activated alumina, alum and brick powder*. Groundwater for Sustainable Development, 7, 452-458.

AHMET, G., SAMIH, B., KEMAL, D., M. SAHIN, G., 1995. *Adsorption of CTAB at lignite-aqueous solution interface*. Fuel Processing Technology, 45(2), 75-84.

BERGINS, C., HULSTON, J., STRAUSS, K., CHAFFEE, A. L., 2007. *Mechanical/thermal dewatering of lignite. Part 3: Physical properties and pore structure of MTE product coals*. Fuel, 86(1-2), 3-16.

CACERES-JENSEN, L., RODRIGUEZ-BECERRA, J., PARRA-RIVERO, J., ESCUDEY, M., BARRIENTOS, L., CASTRO-CASTILLO, V., 2013. *Sorption kinetics of diuron on volcanic ash derived soils*. J Hazard Mater, 261, 602-613.

CHENG, J. Y., WANG, P., MA, J. P., LIU, Q. K., DONG, Y. B., 2014. *A nanoporous Ag(I)-MOF showing unique selective adsorption of benzene among its organic analogues*. Chem Commun (Camb), 50(89), 13672-13675.

DEMIRBAS, A., SARI, A., ISILDAK, O., 2006. *Adsorption thermodynamics of stearic acid onto bentonite*. J Hazard Mater, 135(1-3), 226-231.

GROPPO, J. G., PAREKH, B. K., 1996. *Pilot-Scale Evaluation of Hyperbaric Filtration of Ultra Fine Clean Coal*. Coal Preparation, 17(1-2), 61-70.

HAMEED, B. H., EL-KHAIARY, M. I., 2008a. *Equilibrium, kinetics and mechanism of malachite green adsorption on activated carbon prepared from bamboo by K(2)CO(3) activation and subsequent gasification with CO(2)*. J Hazard Mater, 157(2-3), 344-351.

HAMEED, B. H., EL-KHAIARY, M. I., 2008b. *Kinetics and equilibrium studies of malachite green adsorption on rice straw-derived char*. J Hazard Mater, 153(1-2), 701-708.

HAMEED, B. H., SALMAN, J. M., AHMAD, A. L., 2009. *Adsorption isotherm and kinetic modeling of 2,4-D pesticide on activated carbon derived from date stones*. J Hazard Mater, 163(1), 121-126.

HAO, S. X., LIU, X. Y., YU, Z. X., 2013. *Effect of Deashing Treatment on the Coal Structure and Surface Groups*. Advanced Materials Research, 803, 330-333.

HULSTON, J., FAVAS, G., CHAFFEE, A. L., 2005. *Physico-chemical properties of Loy Yang lignite dewatered by mechanical thermal expression*. Fuel, 84(14-15), 1940-1948.

LE ROUX, M., CAMPBELL, Q. P., WATERMEYER, M. S., DE OLIVEIRA, S., 2005. *The optimization of an improved method of fine coal dewatering*. Minerals Engineering, 18(9), 931-934.

LIU, S., CHEN, M., CAO, X., LI, G., ZHANG, D., LI, M., MENG, N., YIN, J., YAN, B., 2020. *Chromium (VI) removal from water using cetylpyridinium chloride (CPC)-modified montmorillonite*. Separation and Purification Technology, 241, 116732.

LIU, X., LIU, S., FAN, M., ZHANG, L., 2017. *Decrease of hydrophilicity of lignite using CTAB: Effects of adsorption differences of surfactant onto mineral composition and functional groups*. Fuel, 197, 474-481.

LIU, Y., 2009. *Is the Free Energy Change of Adsorption Correctly Calculated.* Journal of Chemical & Engineering Data, 54(7), 1981-1985.

LYU, X., YOU, X., HE, M., ZHANG, W., WEI, H., LI, L., HE, Q., 2018. *Adsorption and molecular dynamics simulations of nonionic surfactant on the low rank coal surface*. Fuel, 211, 529-534.

ONAL, Y., AKMIL-BASAR, C., SARICI-OZDEMIR, C., 2007. *Investigation kinetics mechanisms of adsorption malachite green onto activated carbon*. J Hazard Mater, 146(1-2), 194-203.

OYELUDE, E. O., AWUDZA, J. A. M., TWUMASI, S. K., 2017. *Equilibrium, Kinetic and Thermodynamic Study of Removal of Eosin Yellow from Aqueous Solution Using Teak Leaf Litter Powder*. Sci Rep, 7(1), 12198.

PEDRO SILVA, J., SOUSA, S., RODRIGUES, J., ANTUNES, H., PORTER, J. J., GONçALVES, I., FERREIRA-DIAS, S., 2004. *Adsorption of acid orange 7 dye in aqueous solutions by spent brewery grains*. Separation and Purification Technology, 40(3), 309-315.

SAHA, T. K., KARMAKER, S., ICHIKAWA, H., FUKUMORI, Y., 2005. *Mechanisms and kinetics of trisodium 2-hydroxy-1,1'-azonaphthalene-3,4',6-trisulfonate adsorption onto chitosan*. J Colloid Interface Sci, 286(2), 433-439.

ŞAHIN, S., EMIK, S., 2018. *Fast and highly efficient removal of 2,4-D using amino-functionalized poly (glycidyl methacrylate) adsorbent: Optimization, equilibrium, kinetic and thermodynamic studies*. Journal of Molecular Liquids, 260, 195-202.

SINGH, B. P., 1997. *The influence of surface phenomena on the dewatering of fine clean coal*. Filtration & Separation, 34(2), 159-163.

SINGH, B. P., 1999. *The role of surfactant adsorption in the improved dewatering of fine coal*. Fuel, 78(4), 501-506.

SINGH, B. P., BESRA, L., REDDY, P. S. R., SANGUPTA, D. K., 1998. *Use of surfactants to aid the dewatering of fine clean coal*. Fuel, 77(12), 1349-1356.

SIS, H., CHANDER, S., 2003. *Adsorption and contact angle of single and binary mixtures of surfactants on apatite*. Minerals Engineering, 16(9), 839-848.

STROH, G., STAHL, W., 1990. *Effect of surfactants on the filtration properties of fine particles*. Filtration & Separation, 27(3), 0-199.

SUN, X. F., WANG, S. G., LIU, X. W., GONG, W. X., BAO, N., GAO, B. Y., ZHANG, H. Y., 2008. *Biosorption of Malachite Green from aqueous solutions onto aerobic granules: kinetic and equilibrium studies*. Bioresour Technol, 99(9), 3475-3483.

TAFFAREL, S. R., RUBIO, J., 2009. *On the removal of Mn2+ ions by adsorption onto natural and activated Chilean zeolites*. Minerals Engineering, 22(4), 336-343.

TAO, D., GROPPO, J. G., PAREKH, B. K., 2000. *Enhanced ultrafine coal dewatering using flocculation filtration processes*. Minerals Engineering, 13(2), 163-171.

VADIVELAN, V., KUMAR, K. V., 2005. *Equilibrium, kinetics, mechanism, and process design for the sorption of methylene blue onto rice husk*. J Colloid Interface Sci, 286(1), 90-100.

VAZIRI HASSAS, B., KARAKAŞ, F., ÇELIK, M. S., 2014. *Ultrafine coal dewatering: Relationship between hydrophilic lipophilic balance (HLB) of surfactants and coal rank*. International Journal of Mineral Processing, 133, 97-104.

VOGT, C., WILD, T., BERGINS, C., STRAUß, K., HULSTON, J., CHAFFEE, A. L., 2012. *Mechanical/thermal dewatering of lignite. Part 4: Physico-chemical properties and pore structure during an acid treatment within the MTE process*. Fuel, 93, 433-442.

XIAO, F., YAN, B.-Q., ZOU, X.-Y., CAO, X.-Q., DONG, L., LYU, X.-J., LI, L., QIU, J., CHEN, P., HU, S.-G., ZHANG, Q.-J., 2020. *Study on ionic liquid modified montmorillonite and molecular dynamics simulation*. Colloids and Surfaces A: Physicochemical and Engineering Aspects, 587, 124311.

XU, Y., LIU, Y.-L., HE, D.-D., LIU, G.-S., 2013. *Adsorption of cationic collectors and water on muscovite (001) surface: A molecular dynamics simulation study*. Minerals Engineering, 53, 101-107.

YOON, R.-H., ASMATULU, R., ISMAIL YILDIRIM, JANSEN, W., ZHANG, J., ATKINSON, B., HAVENS, J. (2004). *Development of Dewatering Aids for Minerals And Coal Fines*. Retrieved from United States:

YOU, X., HE, M., CAO, X., WANG, P., WANG, J., LI, L., 2019. *Molecular dynamics simulations of removal of nonylphenol pollutants by graphene oxide: Experimental study and modelling*. Applied Surface Science, 475, 621-626.

YOU, X., HE, M., ZHANG, W., WEI, H., LYU, X., HE, Q., LI, L., 2018. *Molecular dynamics simulations of nonylphenol ethoxylate on the Hatcher model of subbituminous coal surface*. Powder Technology, 332, 323-330.

YOU, X., HE, M., ZHU, X., WEI, H., CAO, X., WANG, P., LI, L., 2019. *Influence of surfactant for improving dewatering of brown coal: A comparative experimental and MD simulation study*. Separation and Purification Technology, 210, 473-478.

ZHOU, Y., ALBIJANIC, B., WANG, Y., YANG, J., 2018. *Characterizing surface properties of oxidized coal using FTIR and contact angle measurements*. Energy Sources, Part A: Recovery, Utilization, and Environmental Effects, 40(12), 1559-1564.

ZHU, B., ZHAO, Z. (1999). *Base of Interface Chemistry*. Beijing: Chemistry Industry Press.

ZHU, X., HE, M., ZHANG, W., WEI, H., LYU, X., WANG, Q., YOU, X., LI, L., 2020. *Formulation design of microemulsion collector based on gemini surfactant in coal flotation*. Journal of Cleaner Production, 257, 120496.

ZHU, X., WEI, H., HOU, M., WANG, Q., YOU, X., LI, L., 2020. *Thermodynamic behavior and flotation kinetics of an ionic liquid microemulsion collector for coal flotation*. Fuel, 262, 116627.